Cepstral Analysis of Photonic Nanojet-Illuminated Biological Cells

César Méndez Ruiz and Jamesina J. Simpson

Department of Electrical and Computer Engineering
University of New Mexico, Albuquerque, NM 87131 USA
cesar.mendez.ruiz@gmail.com, simpson@ece.unm.edu

Abstract ─ It is currently believed that nanometer-scale internal refractive index fluctuations within biological cells change significantly during the initial stages of ultra early-stage cancer development well in advance of these changes becoming more pronounced and histologically detectable. Here, backscattered cepstral results of photonic nanojet-illuminated cells are investigated as a means to offer unique advantages for determining the internal structure and composition of cells at sub-diffraction (nanometer) scales. Specifically, the finite-difference time-domain (FDTD) method is employed to obtain the backscattered cepstrum of photonic-nanojet illuminated human colorectal HT-29 cells. Analysis of the backscattered cepstrum of the HT-29 cells indicates a clear means to distinguish between cells having larger and smaller levels of internal refractive index fluctuations before these changes are histologically detectable. Further, we find that the surface reflection is reduced for the case of nanojet-illuminated cells compared to flat surfaces.

Index Terms ─ Biological media, cancer, cepstrum, FDTD, photonic nanojet.

I. INTRODUCTION

As reported in a 2008 article of the *Proceedings of the National Academy of Sciences* [1], internal refractive index fluctuations are believed to change significantly on a nano-meter scale within biological cells during the initial stages of ultra early-stage cancer development well in advance of these changes becoming more pronounced and histologically detectable. In other words, cellular changes at the nano-meter scale, the scale of some of the fundamental building blocks of cells (such as ribosomes, macromolecular complexes nuceleosomes, membranes, etc.), are expected to be occurring during cancer development in advance of changes at the micro-meter scale. For example, a less aggressive human colorectal cancer cell line (HT-29) is hypothesized in [1] to have 60×60×60 nm correlation lengths, while a more aggressive HT-29 colon cancer cell line is hypothesized to have a correlation length of 600×600×100 nm. In the case of [1], the mean refractive index n_0 of the HT-29 cell is set to 1.38, and the maximum refractive index fluctuation ($\Delta n_{\max}$) is 0.02.

In this paper, HT-29 cells are analyzed in a new way for determining the characteristics of their internal refractive index fluctuations. Specifically, the backscattered cepstrum is obtained for photonic nanojet-illuminated HT-29 cells. This technique of employing the cepstrum as well as a photonic nanojet offers new advantages through unique capabilities for determining the internal structure and composition of cells at sub-diffraction scales. Further, an important advantage of the technique of this paper is that the surface reflection is reduced for cells compared to flat surfaces. This work may thus have application to ultra-early stage cancer detection.

The cepstrum is defined here as taking the discrete Fourier transform (DFT) of the magnitude of the backscattered spectrum:

$$f(t) \rightarrow DFT \rightarrow spectrum$$

$$abs(spectrum) \rightarrow DFT \rightarrow cepstrum$$

The domain of the cepstrum is termed "quefrency" and integer multiples of the fundamental quefrency are termed "rahmonics" [2]. Note that although the units of the

Submitted On: Dec 1, 2011
Accepted On: Feb. 23, 2012

independent variable for the cepstrum is seconds, the cepstrum exists neither in the frequency nor time domain. As for the coining in [2] of the word "cepstra," these terms are formed by reversing the order of the initial letters of their corresponding terms in the frequency domain.

The cepstrum is useful because it permits an analysis of the rate of change and periodicity of the spectrum over the complete frequency range of interest. Let us consider for example a simple recorded backscattered time waveform comprised of multiple reflected pulses having different delays and amplitudes:

$$x(t) = s(t) + \alpha_1 s(t-\tau_1) + \alpha_2 s(t-\tau_2) + \ldots + \alpha_{n_\tau} s(t-\tau_{n_\tau}),$$

where τ_n is the delay of the n^{th} reflection ($\tau_1 < \tau_2 < \ldots < \tau_{n\tau}$), and the α's account for the scaling of the reflections from embedded features within the target as well as the shadow side surface of the target with respect to the magnitude of the reflection from the illuminated side of the target.

The spectrum magnitude of this signal is:

$$|X(f)| = |S(f)| \sqrt{1 + \sum_{i=1}^{n_\tau} \alpha_i^2 + 2\left\{ \sum_{i=1}^{n_\tau} \alpha_i \cos(2\pi\tau_i f) + \sum_{i=1}^{n_\tau - 1} A_i \right\}},$$

where

$$A_i = \alpha_i \alpha_{i+1} \cos\left(2\pi\left[\tau_{i+1} - \tau_i\right] f\right) + \alpha_i \alpha_{i+2} \cos\left(2\pi\left[\tau_{i+2} - \tau_i\right] f\right) + \ldots + \alpha_i \alpha_{n_\tau} \cos\left(2\pi\left[\tau_{n_\tau} - \tau_i\right] f\right)$$

In this case, the cepstrum will be comprised of one peak per feature of the target generating a reflection (each internal feature as well as the shadow-side surface of the target). Each of these cepstral peaks will be located along the x-axis (quefrequency, in units of seconds) at the position corresponding to the difference in round-trip propagation time between the initial reflection from the incident surface of the target and the corresponding reflection from the internal feature / shadow side surface of the target. The magnitudes of all but the last cepstral peak are affected by multiple α values.

A photonic nanojet is defined as a narrow, high-intensity beam of light that emerges from the shadow side of a plane-wave-illuminated dielectric sphere or cylinder of diameter larger than the wavelength, λ [3]. Photonic nanojets have previously been shown to provide sufficiently one-dimensional (1-D) illumination of three-dimensional (3-D) targets [4], yielding the ability to detect at distances of multiple wavelengths in the backscatter direction ultra-subwavelength inhomogeneities embedded within the dielectric targets [4].

In this paper, the cepstral analysis of [4] developed for flat, dielectric slabs is applied to the more complex scenario of HT-29 cells. Here, the backscattered cepstrum is chosen for analysis over the spectrum curve because the target's characteristics are more easily extracted from the cepstral curve than from the periodic backscattered spectrum. Compared to [4], the modeling of this paper is complicated by the surface roughness and overall curvature of the HT-29 cell, as well as by the random internal refractive index fluctuations within the cells. Specifically, the finite-difference time-domain (FDTD) method [5] is employed to obtain the backscattered cepstrum of homogeneous and inhomogeneous HT-29 cells. The 3-D FDTD grids model HT-29 cells, including their surface topography using data from atomic force microscopy (AFM) measurements [6], along with a microsphere for generating the nanojet used to illuminate the HT-29 cells. Analysis of the backscattered cepstrum of the different modeling cases indicates that (1) details of the internal composition of cells are more easily extracted from the backscatter of nanojet-illuminated cells than flat slabs; this could mean detection of smaller and earlier changes in internal refractive index fluctuations; (2) a clear means exists to distinguish between cells having larger and smaller levels of internal refractive index fluctuations before these changes are histologically detectable.

II. 3-D FDTD MODEL DESCRIPTION

First, a healthy HT-29 cell is modeled in the FDTD grid by importing AFM measurement data [6]. AFM can resolve surface fluctuations of lengths on the order of fractions of a nanometer, which is more than 1000 times better than the best resolution obtained using diffraction limited optical systems. Figure 1 illustrates a top-down view of the topography of the HT-29 cell that is imported to the FDTD model. The HT-29 cell is modeled as being submerged in water, which permits studying living cells instead of dehydrated cells. Note that it is modeled here as being stationary in the FDTD grid.

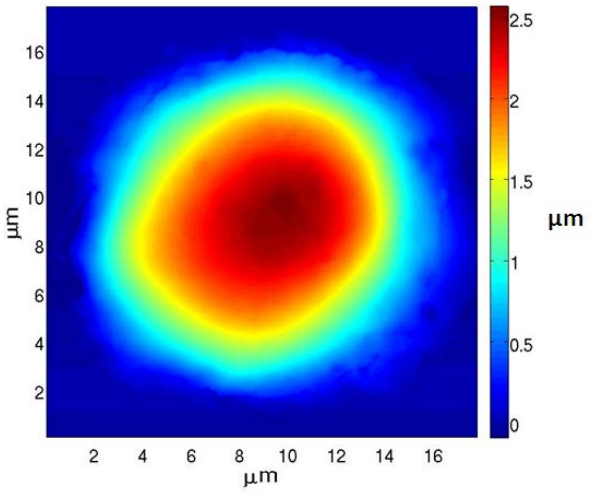

Fig. 1. AFM surface topography of a fixed human colorectal HT-29 cell, courtesy of Dr. Richter [6]. 512 sampling points are collected in each direction over a 17.8 by 17.8 μm area providing a resolution of ~3.48 nm Nanowizard II (JPK Instruments AG, Germany), uncoated NSG10 tip (NT-MDT, Russia).

Next, a 1.5-μm diameter silica sphere having a refractive index n of 1.42 is modeled in a FDTD grid. This microsphere produces a photonic nanojet as shown in Fig. 2 that is later used to probe the HT-29 cell of Fig. 1. Note that the microsphere is also submerged in water, leading to an entire microsphere-HT-29 cell system that is submerged in water. Submerging the nanojet-generating microsphere improves the length of the nanojet and also reduces unintended resonances inside the sphere due to the lower refractive index contrast of the silica sphere with water rather than free space.

In subsequent simulations, the sphere center is located 950 nm from the top (incident side) surface of the HT-29 cell. A total-field scattered-field FDTD formulation [5] is employed to illuminate the microsphere with a plane wave, which then yields the nanojet for probing the HT-29 cell. For each simulation case, the backscattered time-waveform is recorded 3.8 μm on the incident side of the microsphere for subsequent post-processing. Note that as part of the post-processing, the time-domain backscatter from the microsphere alone is subtracted from case of the microsphere plus HT-29 cell case. This permits better extraction of the backscattered signal from the HT-29 cell.

Finally, the FDTD grid unit cell size is set to 10 nm in each Cartesian direction. This value is chosen not based on the Courant limit [5], but rather from the fine details of the cell surface topography. The spacing between measuring points (in x and y directions) in the provided AFM traces is 34.8 nm, but the vertical (z-direction) resolution of AFM is on the order of fractions of a nanometer. As such, starting with a grid cell size of 30 nm, iterative FDTD simulations involving the nanojet and the homogeneous HT-29 cell (n_0 = 1.38) while using progressively smaller FDTD grid cell sizes were run until convergence of the backscattered waveform was achieved at a grid resolution of 10 nm.

III. FDTD MODELING RESULTS

A. Homogeneous case

First, the HT-29 cell of Fig. 1 is modeled as having a homogeneous permittivity of 1.38 and as being illuminated by the nanojet of Fig. 2 at its geometric center. Note from Fig. 1 that the geometric center of the cell does not correspond to its peak thickness, which is slightly off-center and to the upper right of the central point. Also, the cell AFM topography is modeled only on the front side of the illuminated cell, and the shadow-side surface of the cell is modeled as being flat. Although modeling the two-sided surface topography of the HT-29 cell would be more realistic, here, having a flat shadow side HT-29 cell provides a useful comparison of the effects of the front (AFM surface data) side and back (flat) sides of the cell on the backscattered signal.

Figure 3 illustrates the time-domain backscattered waveform of the nanojet-illuminated HT-29 cell. Also shown for comparison is the backscattered waveform of a homogeneous slab of the same n and same average thickness as the HT-29 cell (as measured from Fig. 1 only over the transverse circular area of the cell illuminated by the nanojet). The results of Fig. 3 show for both the cell / slab cases two pulses occurring together in time, and representing the reflections from the front and back sides of the cell / slab. Since the shadow-side surface of both the cell and the slab are flat, the second pulses are nearly identical for both cases. The earlier reflection from the front side, however, indicates a lower amplitude reflection from the cell compared to that of the slab. This is due to the surface topology and

roughness of the cell, which scatters the incident wave in more directions than just directly backward as is the case for the flat slab.

As a result, from the results of Fig. 3, we find that an important advantage of the technique of this paper involving nanojets and the analysis of backscattered waveforms from biological cells, is that the surface reflection is reduced for cells compared to flat surfaces. This means that inhomogeneities within HT-29 cells, for example, such as internal refractive index fluctuations hypothesized to occur during the initial stages of cancer development, are more easily detectable in HT-29 cells compared to flat slabs, since the surface reflections of the cells are reduced in the backscattered direction. Further, cells having rougher or more drastically curved surfaces will permit even better detection of the internal composition of the cells. We note that a question not addressed in [1] is whether early-stage cancer is detectable by characterizing changes in the surface topology of biological cells rather than or in addition to the internal refractive index changes [7]. The technique of this paper could help answer this question.

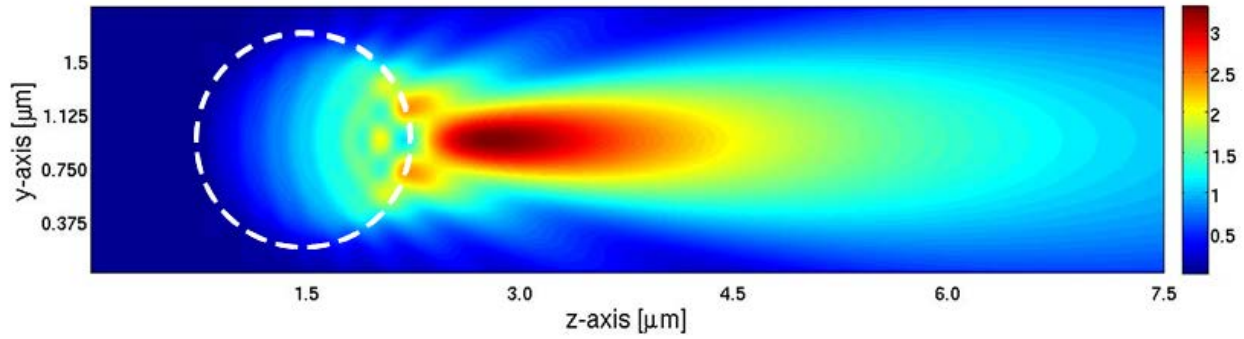

Fig. 2. Visualization of a photonic nanojet generated by a plane-wave-illuminated, 1.5-μm diameter silica microsphere submerged in water. The single frequency incident light λ is 500 nm. The steady-state electric field amplitude is plotted.

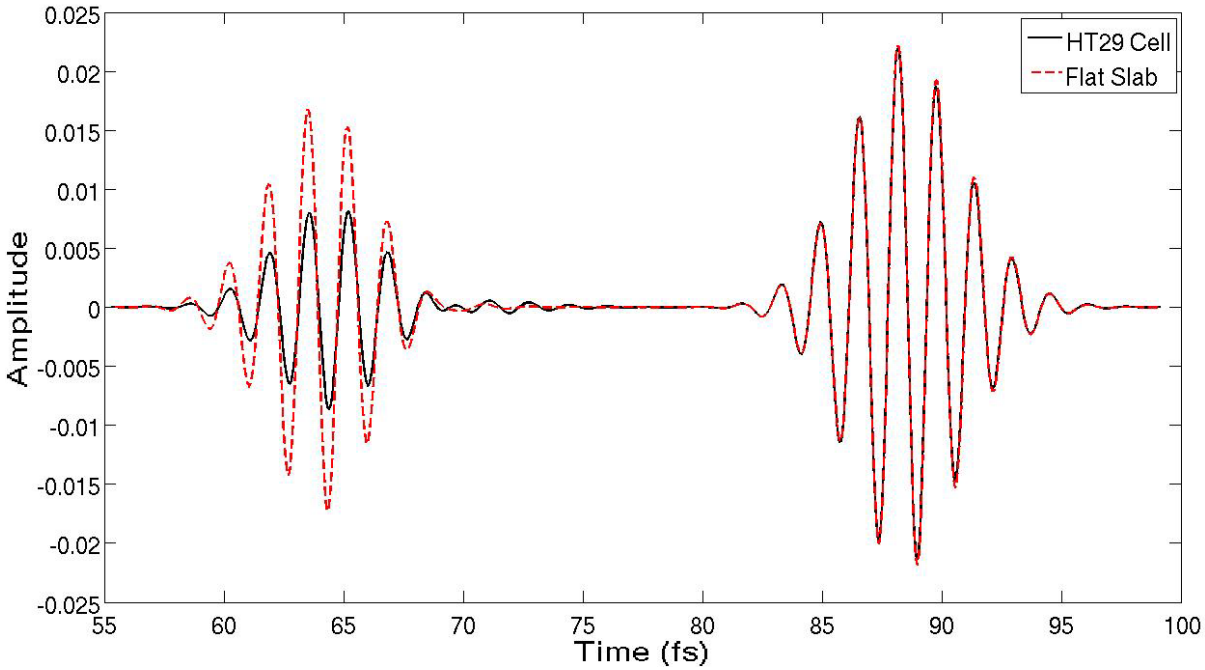

Fig. 3. Recorded time-domain backscatter from the HT-29 cell, and a dielectric slab having the same *n* and average thickness. The source is a Gaussian of half-width 3.18 fs modulating a sinusoid at 500 nm center wavelength.

B. Inhomogeneous case

Next, the HT-29 cell is modeled as having a pseudorandom *n* pattern. Fluctuations of the *n* inside of cells can arise due to varying concentrations of intracellular solids like DNA, RNA, lipids, etc. As a result, here, the intra cellular solids of the biological cell are modeled as a stationary process in the second-order cumulant approximation [8], as was done in the work of [1]. For this approximation, the *n* is determined to vary randomly with position but is held constant (homogeneous) within each block of dimension equal to a parameter termed the correlation length, *lc*. That is, the correlation function (the correlation between random variables, in this case refractive index values, at positions in space and as a function of the spatial distance between those two points) is defined by

$$\gamma(r) = \left\langle n(r_i) \cdot n(r_j) \right\rangle_r / \left\langle n^2 \right\rangle$$

where $\left\langle n^2 \right\rangle$ denotes the mean-square average of the fluctuation of the refractive index and $\left\langle n(r_i) \right\rangle$ and $\left\langle n(r_j) \right\rangle$ are the fluctuations of the refractive index at *i* and *j* positions that are a distance *r* apart. The correlation function varies from 0 when *r* is very large to 1 when *r*=0. For a random distribution of refractive index values, the correlation function can be approximated by [9]:

$$\gamma(r) = \exp\left(\frac{-r}{l_c}\right).$$

In our case, the value of *n* for each homogeneous block is determined pseudorandomly, and we choose to investigate the effects of different size blocks similar to those considered in [1]. Specifically, the *lc* value corresponds to the size of the intracellular structures within a cell, and is currently hypothesized to correlate with the cancer aggressiveness level of the cell [1]. As a result, the *lc* value is changed for the different HT-29 cells corresponding to different levels of cancer development. On the other hand, the maximum *n* variations (Δn) is proportional to the local concentration of intracellular solids. Here, for all simulation cases, the mean refractive index n_o is equal to 1.38 as in [1]. The Δn for typical biological tissue can range from 0.02 to 0.1 [10]; for this work, the maximum Δn is set to 0.1.

Figure 4 shows an example 2-D geometry slice of a 3-D FDTD grid for the case of the HT-29 cell filled with 60×60×60 nm *n* blocks, along with the microsphere for generating the nanojet.

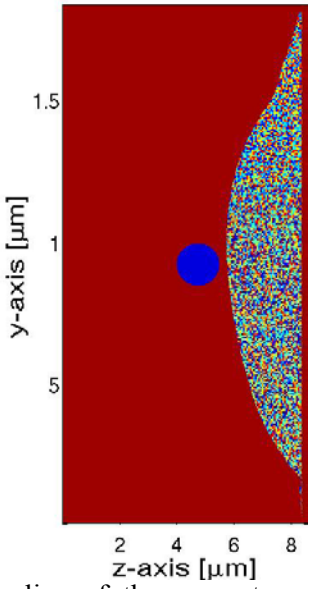

Fig. 4. 2-D slice of the geometry of the silica microsphere for generating the nanojet along with the HT-29 cell having a 60×60×60 nm pseudorandom *n* pattern.

Note that to date (as mentioned at the end of Section 3A), a systematic study of any changes possibly occurring in the cell topography during cancer development has not yet been performed. As a result, we also assume here for the inhomogeneous HT-29 cells corresponding to different levels of cancer aggressiveness the same cell topography obtained for a healthy HT-29 cell and used in Section 3A. This is because AFM topography data for HT-29 cells at different levels of cancer aggressiveness is not readily available. But we note that obtaining such data would be an important part of future work in order to understand what important changes, if any, are occurring at the cell surface during advancement of the cancer.

In the first of two studies involving random *n* fluctuations within HT-29 cells, the sensitivity of the backscatter signal due to different *lc* values is tested. Specifically, separate FDTD simulations are run involving nanojet-illuminated HT-29 cells having a pseudorandom *n* composition with homogeneous block sizes of 600×600×100 nm, 60×60×60 nm, 30×30×30 nm, and 10×10×10 nm.

The resulting cepstral curves for each case are shown in Fig. 5.

In general, the magnitude of the cepstrums in Fig. 5 indicates that a decrease of the *lc* leads to a reduction of the total backscattered energy from the cell, especially for quefrequencies above 0 fs corresponding to the initial reflection from the incident-side surface of the cell. That is, the quefrency corresponds to the delay time between the initial reflection (at 0 fs) and subsequent reflections, so a reduction between the different pseudorandom *n* cases of the magnitude between 0 and 25 fs indicates less reflection from the internal *n* blocks (a directly backscattered reflection from the shadow-side surface would occur at 25 fs). In fact, as we may expect, as the *n* blocks reduce in size, the cepstral curve converges to the case of the cell being completely homogeneous. Before this convergence, however, Fig. 5 indicates that *n* blocks as small as about 30 nm can be detected in the cepstral curve, demonstrating the nanojet's potential to detect the fundamental "building blocks" of biological cells (nucleosomes, protein complexes, cytoskeleton, etc.) that have been experimentally shown to be on the order of ~100 nm or less [1].

The maximum magnitude variation of the *n* inside the biological cell is a constant that does not depend on how advanced the carcinogenesis stage is; what determines the aggressiveness of a cell line and distinguishes it from other lines is the value of *lc* [1]. As such, in the second study involving random *n* fluctuations within HT-29 cells, two cases of cell lines are considered. One is the C-terminal Src kinase (Csk) knockdown that is represented with 600×600×100 nm rectangular homogeneous *n* blocks. The other case is the epidermal growth factor receptor (EGFR) knockdown which is less aggressive and is represented with 60×60×60 nm *n* blocks [1]. The cepstral curves from three different pseudorandom patterns per cell line are shown in Fig. 6.

In general, the more aggressive cell line (CsK) backscatters more energy than the EGFR line, but above 5 fs it is insufficient to examine the cepstral curves and unambiguously distinguish between the two cell lines. On the other hand, for all six cases, it is possible to distinguish one cell line from the other based on the magnitude at quefrency 0 fs (higher magnitudes for all three CsK cases, and lower magnitudes for all three EGFR cases). This indicates the possibility of using a cepstral analysis of the backscatter from nanojet-illuminated cells to determine the aggressiveness of cancer cells at sub-diffraction scales and before the disease provokes alterations detectable using histological techniques.

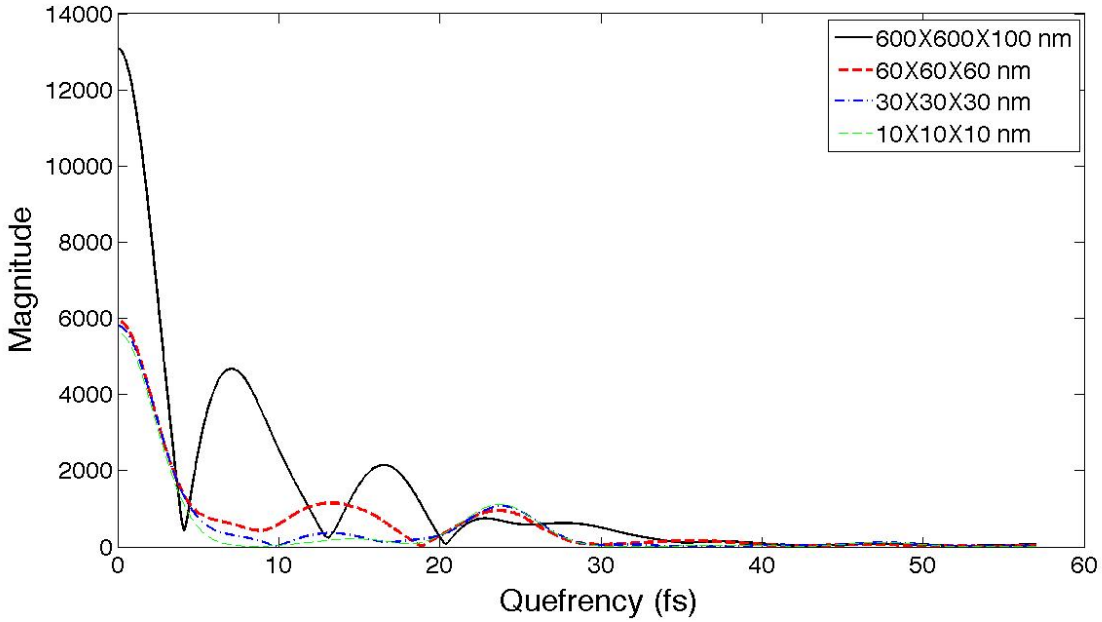

Fig. 5. Comparison of cepstral curves for HT-29 cells having n blocks of different sizes. The homogeneous case is not shown because it is a perfect match with the 10×10×10 nm blocks.

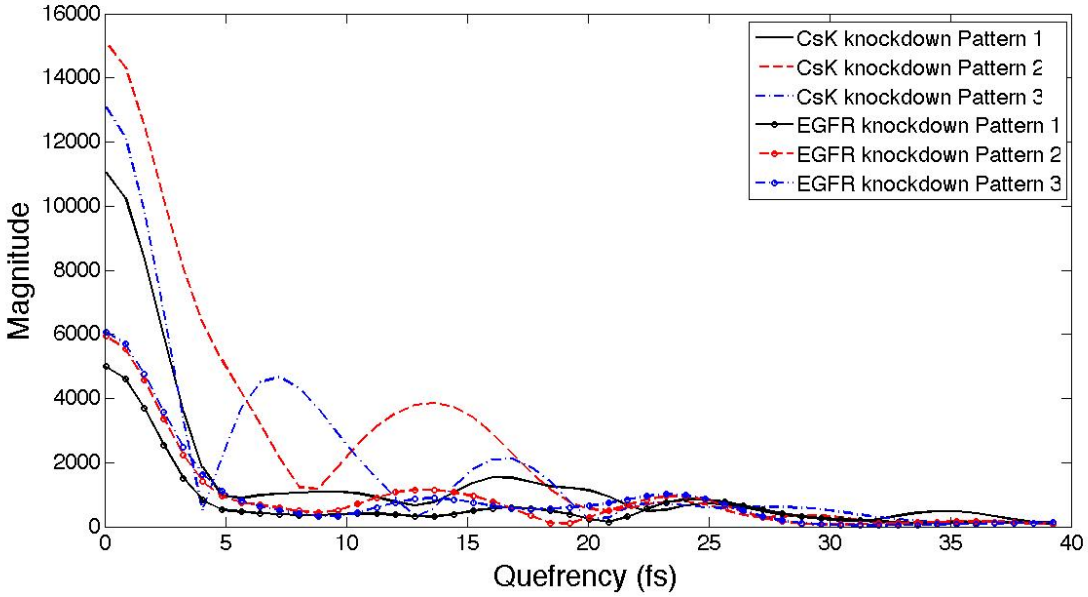

Fig. 6. Comparison of cepstral curves from CsK and EGFR cell lines. Results for three pseudorandom internal *n* fluctuation patterns are shown for each cell line.

Note again that the magnitudes at quefrequency 0 fs in all the figures of this paper, including Fig. 6, correspond to the reflection from the incident surface of the cell, whereas the larger quefrequency values correspond to later reflections involving the internal fluctuations within the cells.

IV. CONCLUSIONS AND ONGOING WORK

Analysis of the backscattered cepstrum of the photonic nanojet-illuminated HT-29 cells has demonstrated that (1) details of the internal composition of cells are more easily extracted from the backscatter of nanojet-illuminated cells than flat slabs; this could aid the detection of smaller and earlier changes in the internal refractive index fluctuations; (2) a clear means exists to distinguish between cells having larger and smaller levels of internal refractive index fluctuations before these changes are histologically detectable.

The study presented in this paper relates to a wide variety of other work being performed by other groups involving the interaction of electromagnetic waves with biological tissues and cells [11 – 13].

As part of future work, laboratory measurements will be conducted to support the computational results of this paper. This will include comprehensive AFM measurements of HT-29 cells at different stages of cancer development in order to help address the question not answered in [1]: whether early-stage cancer is detectable by characterizing changes in the surface topology of biological cells rather than or in addition to the internal refractive index changes. The use of photonic nanojets and the cepstrum may be particularly useful in answering this question, since changes in the surface topography from flatter and smoother to more curved and rough provides noticeably better detection of the internal composition of the cells.

ACKNOWLEDGMENT

This work was supported by the Engineering Research Centers Program of the National Science Foundation under NSF Cooperative Agreement No. EEC-0812056. Also, CONACYT Fellowship number 304287 supported author C. Méndez Ruiz's (209576) graduate studies. Supercomputing resources were provided by the New Mexico Computing Applications Center and the University of New Mexico's Center for Advanced Research Computing (CARC).

REFERENCES

[1] H. Subramanian, P. Pradhan, Y. Liu, I. Capoglu, X. Li, J. Rogers, A. Heifetz, D. Kunte, H. Roy, A. Taflove, and V. Backman, "Optical Methodology for Detecting Histologically Unapparent Nanoscale Consequences of Genetic Alterations in Biological Cells," *Proc. Natl. Acad. Sci*., vol. 105, issue 51, pp. 20124-20129, 2008.

[2] B. P. Bogert, M. J. R. Healy, J. W. Tukey, and M. Rosenblatt, "The Quefrency Analysis of Time Series for Echoes: Cepstrum, Pseudo-Autocovariance, Cross-Cepstrum, and Saphe Cracking," *in Time Series Analysis*, M. Rosenblatt, Ed., ch. 15, pp. 209–243, 1963.

[3] A. Heifetz, S.-C. Kong, A. V. Sahakian, A. Taflove, and V. Backman, "Photonic Nanojets," *J. Computational & Theoretical Nanoscience*, vol. 6, pp. 1979-1992, Sept. 2009.

[4] C. Méndez Ruiz and J. J. Simpson, "Detection of Embedded Ultra-Subwavelength-Thin Dielectric Features using Elongated Photonic Nanojets," *Optics Express*, vol. 18, iss. 16, pp. 16805-16812, 2010.

[5] A. Taflove and S. C. Hagness, Computational Electrodynamics: The Finite-Difference Time-Domain Method, 3rd edition. Norwood, MA: Artech House, 2005.

[6] Personal communications with Dr. Marc Richter of the Institute of Photonic Technology in Jena, Germany.

[7] P. Pradhan, D. Damania, H. M. Joshi, V. Turzhitsky, H. Subramanian, H. K. Roy, A. Taflove, V. P. Dravid, and V. Backman, "Quantification of Nanoscale Density Fluctuations Using Electron Microscopy: Light-Localization Properties of Biological Cells," *Phys. Biol.*, vol. 8, issue 2, 2011.

[8] S.B. Haley and P. Erdos, "Wave-Propagation in One-Dimensional Disordered Structures," *Phys Rev B*, vol. 45, issue 15, pp. 8572–8584, 1992.

[9] P. Debye, H. R. Anderson, Jr., and H. Brumberger, "Scattering by an Inhomogeneous Solid. II. The Correlation Function and Its Application," *Journal of Applied Physics*, vol. 28, no. 6, pp. 679 – 683, 1957.

[10] J. M. Schmitt and G. Kumar, "Optical Scattering Properties of Soft Tissue: A Discrete Particle Model," *Appl. Opt.*, vol. 37, issue 13, pp. 2788-2797, 1998.

[11] D. A. Woten and M. El-Shenawee, "Quantitative Analysis of Breast Skin for Tumor Detection Using Electromagnetic Waves," *Applied Computational Electromagnetics Society (ACES) Journal*, vol. 24, no. 5, pp. 458 – 463, October 2009.

[12] M. A. Eleiwa and A. Z. Elsherbeni, "Debye Constants for Biological Tissues From 30 Hz to 20 GHz," *Applied Computational Electromagnetics Society (ACES) Journal*, vol. 16, no. 3, pp. 202 – 213, November 2001.

[13] S. Caorsi, E. Bermani, and A. Massa, "A Microwave Imaging Approach Based on Amplitude-Only Data for the Reconstruction of the Electromagnetic Field Induced in Biological Phantoms," *Applied Computational Electromagnetics Society (ACES) Journal*, vol. 16, no. 2, pp. 79 – 89, July 2001.

César Méndez Ruiz was born in México City, México, on June 1, 1980. He received the B.S. diploma in Electromechanical Engineering from the Universidad Panamericana, Zapopan, Jalisco, México, in 2003, the M.S. degree in Electronic Engineering from the Universidad de Guadalajara, Guadalajara, Jalisco, México, in 2007, and the Ph.D. degree in Electrical Engineering from the University of New Mexico, Albuquerque, NM, USA.

From 2002 to 2003, he was a trainee in Hewlett-Packard (HP). He has professional experience in R&D area working as a mechanical design engineer for HP and Best in Development and Technology (BDT). Currently he is employed at Intel Corporation, Guadalajara, Mexico.

Jamesina J. Simpson received the B.S. and Ph.D. degrees in Electrical Engineering from Northwestern University, Evanston, IL, in 2003 and 2007, respectively. As a graduate student, Dr. Simpson was a recipient of the National Science Foundation Graduate Research Fellowship and the IEEE AP-S and MTT-S Research Awards.

In 2007, Dr. Simpson joined the Electrical and Computer Engineering Department at the University of New Mexico – Albuquerque as a tenure-track Assistant Professor. Her research lab encompasses the application of the full-Maxwell's equations finite-difference time-domain (FDTD) method to model a wide variety of scientific and engineering applications. In 2010, Dr. Simpson received an NSF CAREER award.